

The twofold diabaticization of the $\text{KRb } (1 \sim 2)^1\Pi$ complex in the framework of *ab initio* and deperturbation approaches

S. V. Kozlov, E. A. Pazyuk, A. V. Stolyarov

Department of Chemistry, Lomonosov Moscow State University, 119991 Moscow, Leninskie gory 1/3, Russia

(Dated: 2 August 2016)

We performed a diabaticization of the mutually perturbed $1^1\Pi$ and $2^1\Pi$ states of KRb based on both electronic structure calculation and direct coupled-channel deperturbation analysis of experimental energies. The potential energy curves (PECs) of the diabatic states and their scalar coupling were constructed from the *ab initio* adiabatic PECs by analytically integrating the radial $\langle \psi_1^{ad} | \partial / \partial R | \psi_2^{ad} \rangle$ matrix element obtained by a finite-difference method. The diabatic potentials and electronic coupling function were refined by the least squares fitting of the rovibronic termvalues of the $1^1\Pi \sim 2^1\Pi$ complex. The empirical PECs combined with the coupling function as well as the diabaticized spin-orbit coupling and transition dipole matrix elements are useful for further deperturbation treatment of both singlet and triplet states manifold.

I. INTRODUCTION

The accurate representation of the interacting electronic states plays a key role in understanding the detailed mechanism of the photo and collisionally induced chemical reactions. The singlet-triplet levels of alkali metal dimers serve as an intermediate state in the two step optical transformation of the weakly bound atomic pairs into the absolute ground $X^1\Sigma^+(v=0, J=0)$ molecular state^{1,2}. To suppress the undesired spontaneous transitions to the low-lying states a coherent stimulated Raman adiabatic passage³ (STIRAP) is often used.

The photoassociative production and trapping of ultracold KRb molecules has been performed⁴. The resonance coupling of the $B(1)^1\Pi$ and $2^1\Pi$ states of KRb (see, Fig. 1) is found to be a promising pathway for direct photoassociative formation of the $X(0,0)$ ultracold molecules⁵. The rigorous multi-channel modeling of the laser formation of vibrationally cold KRb molecules has been accomplished in Ref. 6. The $a^3\Sigma^+ \rightarrow A^1\Sigma^+ \sim b^3\Pi \rightarrow X^1\Sigma^+$ and $a^3\Sigma^+ \rightarrow B^1\Pi \sim c^3\Sigma^+ \rightarrow X^1\Sigma^+$ optical schemes to create ultracold KRb molecules have been studied⁷ by using the *ab initio* potential energy curves (PECs), spin-orbit coupling (SOC) and transition dipole moment (TDM) functions. The combination of a molecular beam (MB) and an ultracold molecule (UM) excitation spectroscopy⁸ was used to identify the optimal $a^3\Sigma^+(v''_a=21) \rightarrow B^1\Pi(v'_1=8) \rightarrow X^1\Sigma^+(v''_X=0)$ STIRAP pathway for the $^{39}\text{K}^{85}\text{Rb}$ molecule assembling. The magnetoassociated fermion $^{40}\text{K}^{87}\text{Rb}$ molecules have been STIRAP transferred^{9,10} to the lowest $X(0,0)$ level through the $B^1\Pi \sim c^3\Sigma^+$ levels located near the second dissociation threshold.

A comprehensive review of modern spectroscopic studies of the KRb electronic states can be found in the e-book¹². The mutually perturbed $1^1\Pi$ and $2^1\Pi$ states converging to the second $\text{K}(4^2\text{S})+\text{Rb}(5^2\text{P})$ and third $\text{K}(4^2\text{P})+\text{Rb}(5^2\text{S})$ dissociation thresholds were investigated^{13,14} using Doppler-free optical-optical double resonance polarization spectroscopy (OODRPS). In the sub-

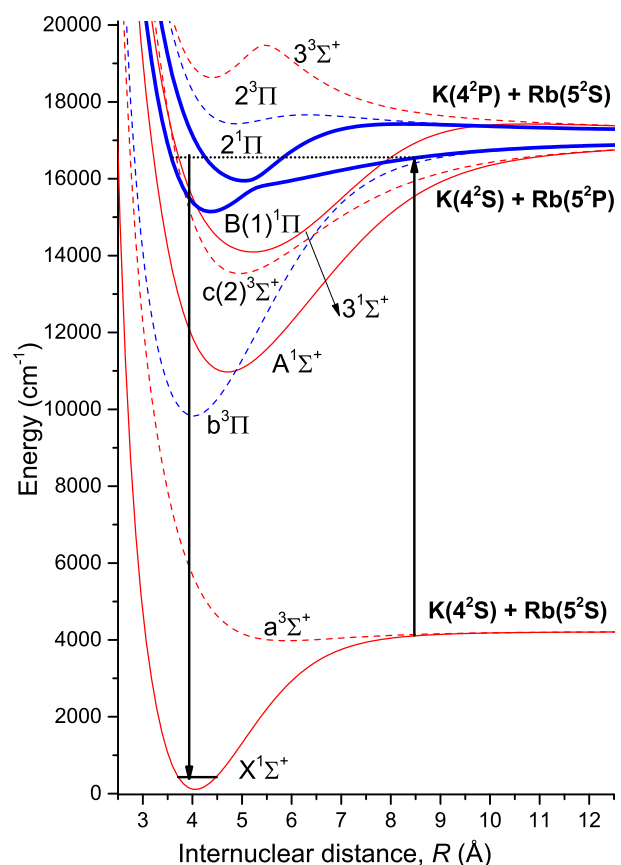


FIG. 1. Scheme of the *ab initio* adiabatic potential energy curves¹¹ of the KRb electronic states correlated to the lowest three dissociation limits. The arrows denote a possible two step stimulated Raman adiabatic passage⁹.

sequent laser induced $3^1\Pi \rightarrow 2^1\Pi$ fluorescence (LIF) studies^{15,16} of both $^{39}\text{K}^{85}\text{Rb}$ and $^{39}\text{K}^{87}\text{Rb}$ isotopologues by Fourier transform spectroscopy (FTS) the vibrational numbering of the $2^1\Pi(v'_2)$ state was corrected by 6 vibrational quanta. The experimental rovibronic term values

of the $1^1\Pi \sim 2^1\Pi$ complex were reduced to the "effective" band $E_{v'}$, $B_{v'}$ and conventional Dunham Y_{ij} molecular constants^{14,15}. The Rydberg-Klein-Rees (RKR) potential was constructed for the adiabatic $B(1)^1\Pi$ state (see, Fig. 2). The vibrational termvalues of the lowest $B^1\Pi(v'_1 \in [0, 21])$ levels were obtained during the spectroscopic analysis of the MB experiment¹⁷. The ground singlet $X^1\Sigma^+$ and triplet $a^3\Sigma^+$ states were comprehensively studied by means of high resolution LIF spectra¹⁸ coming from the spin-orbit coupled $B^1\Pi \sim c^3\Sigma^+$ levels.

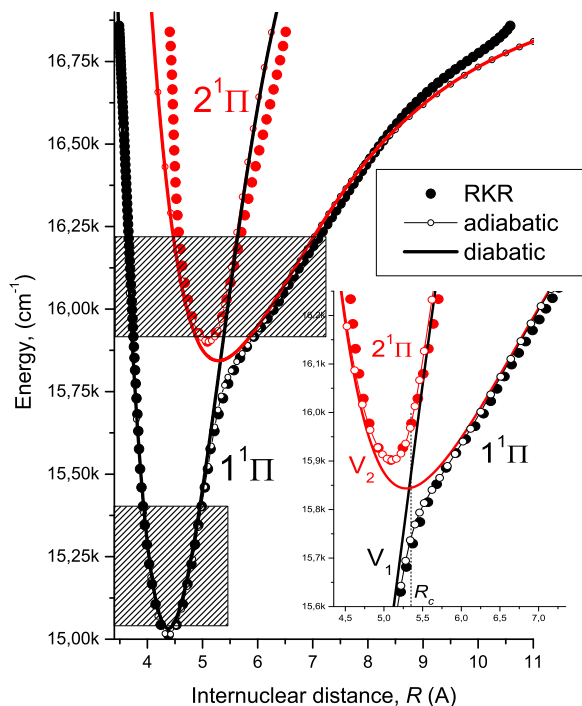


FIG. 2. The empirical adiabatic (open symbols - present work, closed symbols - RKR) and diabatic (solid lines) PECs available for the $(1, 2)^1\Pi$ twin states of KRB. The RKR potential for the $2^1\Pi$ state was built using the Dunham coefficients¹⁵, while the RKR points of the $B(1)^1\Pi$ state were borrowed from Ref. 14. The shadowed regions indicate the rovibronic $E_{v'J'}$ termvalues data sets^{15,16} included in the present CC deperturbation analysis. The inset enlarges the region in the vicinity of the crossing point of $V_1(R)$ and $V_2(R)$ diabatic PECs.

The adiabatic potentials, permanent and transition dipole moments for the radially coupled $1^1\Pi$ and $2^1\Pi$ states were first *ab initio* calculated in Refs 19 and 20. The comprehensive set of non-relativistic PECs, permanent and transition dipole moments for the ground and excited states of KRB are available^{11,21–25} as well. The SOC effect has been included into *ab initio* calculations in Refs. 6, 11, 24, and 26.

Among other alkali diatomics, the KRB molecule stands out because of the high density of the electronic states belonging to both singlet and triplet manifolds. This is attributed to the accidental close values of the ionization potential, electronic affinity and the polarizability of K and Rb atoms in their ground states as well as the almost degenerate energies of the first excited K(4^2P) and Rb(5^2P) states^{27–29}. The high density of the low-lying covalence and ion-pair states apparently leads to the pronounced radial coupling effect between the states of the same spatial and spin symmetry. This appears (see, for example, Figs. 1 and 2) as an avoided crossing of the corresponding adiabatic PECs as well as a sharp dependence of the relevant electronic matrix elements on the internuclear distance R . The sharp R -dependence of the spin-orbit, angular and radial coupling matrix elements embarrasses a deperturbation analysis while the abrupt R -variation of the adiabatic TDM functions prevents to a straightforward simulation of radiative properties.

The electronic coupling matrix element $V_{12} \approx U_1(R_c) - U_2(R_c)$ estimates near the avoided crossing point R_c of the adiabatic PECs warn that a conventional adiabatic approximation is not ideally suitable for representation of the twin $(1, 2)^1\Pi$ states of KRB, since the so-called adiabaticity parameter³⁰ $\gamma \equiv V_{12}/\sqrt{\omega_1\omega_2}$ is close to 3. Here, ω_i are harmonic frequencies of the interacting adiabatic states. To our best knowledge, a global deperturbation analysis of the $1^1\Pi \sim 2^1\Pi$ complex has not been performed yet in the framework of either adiabatic or diabatic approximation.

In the present work, we performed a twofold diabaticization of the KRB $1^1\Pi \sim 2^1\Pi$ complex by means of mutually complementary methods, namely: *ab initio* electronic structure calculations and direct coupled-channel (CC) deperturbation treatment of experimental termvalues^{12–17}.

II. AB INITIO DIABATIZATION OF THE $(1 \sim 2)^1\Pi$ TWIN STATES

The simplest two-state transformation (diabatization) of the adiabatic electronic wavefunctions $\psi_{1,2}(R)$ to their diabatic counterparts $\varphi_{1,2}(R)$ can be realized by the unitary transformation³⁰

$$\begin{pmatrix} \varphi_1 \\ \varphi_2 \end{pmatrix} = \begin{pmatrix} \cos \theta & \sin \theta \\ -\sin \theta & \cos \theta \end{pmatrix} \begin{pmatrix} \psi_1 \\ \psi_2 \end{pmatrix} \quad (1)$$

where the rotation angle $\theta(R)$ is evaluated as a function of the internuclear distance R by integration of the radial coupling matrix element:

$$B_{12} \equiv \langle \varphi_1 | \partial / \partial R | \varphi_2 \rangle = \frac{d\theta}{dR}. \quad (2)$$

The integration of the *ab initio* calculated radial coupling matrix element (2) is performed implicitly by means of a smooth interpolation of the original point-wise $B_{12}(R)$ function in the vicinity of a dominant maximum (which

is located near the avoided crossing point R_c of the corresponding adiabatic potentials) by the simplest Lorentz form³⁰:

$$B_{12}(R) \approx \frac{w}{4(R - R_c)^2 + w^2} \quad (3)$$

with the two R -independent parameters R_c and w . Then, the required rotation angle function

$$\theta(R) = \frac{1}{2} \arctan \left[\frac{2(R - R_c)}{w} \right] + \frac{\pi}{4} \quad (4)$$

is prolonged to the $R \in [0, +\infty)$ -range in order to accomplish a diabaticization of the corresponding electronic wave functions (1).

The diabatic potentials $V_{1,2}(R)$ and electronic coupling matrix element $V_{12}(R)$ are calculated from the adiabatic PECs $U_{1,2}(R)$ via the relations:

$$\begin{aligned} V_1 &= \cos^2 \theta U_1 + \sin^2 \theta U_2 \\ V_2 &= \sin^2 \theta U_1 + \cos^2 \theta U_2 \\ V_{12} &= \sin 2\theta |U_1 - U_2|/2 \end{aligned} \quad (5)$$

The adiabatic PECs $U_i^{ab}(R)$ were evaluated for the low-lying excited $(1-3)^{1,3}\Sigma^+$ and $(1,2)^{1,3}\Pi$ states converging to the lowest three dissociation limits (see Fig. 1) in the basis of the zeroth-order (spin-averaged) electronic wavefunctions corresponding to pure (a) Hund's coupling case. To diminish the systematic R -dependent error (first of all, basis set superposition error) the originally calculated adiabatic potentials U_i^{ab} for the excited states were corrected due to the semi-empirical relation²:

$$U_i(R) = [U_i^{ab}(R) - U_X^{ab}(R)] + U_X^{emp}(R) \quad (6)$$

where the highly accurate empirical PEC U_X^{emp} of the ground $X^1\Sigma^+$ state was borrowed from Ref. 18.

All electronic structure calculations were performed in a wide range of internuclear distances on the density grid by means of the MOLPRO program package³¹. The radial coupling matrix element $B_{12}(R)$ between the $1^1\Pi$ and $2^1\Pi$ states was evaluated by three points finite-difference method.

The details of the computational procedure used can be found elsewhere²⁴. Briefly, the inner core shell of both potassium and rubidium atoms was replaced by energy-consistent non-empirical effective core potentials³² (ECP), leaving 9 outer shell (8 sub-valence plus 1 valence) electrons for explicit treatment. The relevant spin-averaged and spin-orbit Gaussian basis sets used for each atom (ECP10MDF for K and ECP28MDF for Rb, respectively) were taken from the above reference. The optimized molecular orbitals were constructed from the solutions of the state-averaged complete active space self-consistent field problem for all 18 electrons on the lowest $(1-10)^{1,3}\Sigma^+$ and $(1-5)^{1,3}\Pi$ electronic states taken with equal weights³³. The dynamical correlation was introduced via the internally contracted multi-reference configuration interaction (MRCI) method³⁴ which was applied for only two valence electrons keeping the remaining 16 sub-valence electrons frozen. The l -independent

core-polarization potentials (CPPs) of both atoms (see Table I) were employed to implicitly account for the residual core-valence correlation effects³⁵. The corresponding CPP cut-off radii of both atoms were adjusted to reproduce the experimental fine-structure splitting of the lowest excited K(4^2P) and Rb(5^2P) states²⁹.

TABLE I. The static dipole polarizability²⁸ of the cation and its cut-off radii implemented in the CPP potentials of the K and Rb atoms. All parameters in *a.u.*

	α_{core}	$r_{cut-off}$
K	5.354	0.247
Rb	9.096	0.379

The resulting MRCI wave functions were used to evaluate the permanent dipole functions $d_{1,2}(R)$ of adiabatic $1^1\Pi$ and $2^1\Pi$ states as well as the corresponding $1^1\Pi - 2^1\Pi$ transition dipole moment $d_{12}(R)$. The adiabatic matrix elements were transformed to the relevant diabatic moments $\mu_{1,2}(R)$, $\mu_{12}(R)$ as

$$\begin{aligned} \mu_1 &= \cos^2 \theta d_1 + \sin^2 \theta d_2 - \sin 2\theta d_{12} \\ \mu_2 &= \sin^2 \theta d_1 + \cos^2 \theta d_2 + \sin 2\theta d_{12} \\ \mu_{12} &= \cos 2\theta d_{12} + \sin 2\theta |d_1 - d_2|/2 \end{aligned} \quad (7)$$

Finally, we have calculated spin-orbit $\xi_{ij}(R)$ ($j \in (1,2)^3\Pi; (2,3)^3\Sigma^+$) and angular $L_{ij}^\pm(R)$ ($j \in (1-3)^1\Sigma^+$) coupling matrix elements as well as transition dipole moments $d_{ij}(R)$ ($j \in (1,2)^1\Sigma^+$) for adiabatic $i \in 1^1\Pi, 2^1\Pi$ states. The resulting adiabatic matrix elements $W_{ij} \in \xi_{ij}, L_{ij}^\pm, d_{ij}$ were unitary transformed to their diabatic counterparts W_{ij} as

$$\begin{aligned} W_{1j} &= \cos \theta W_{1j} + \sin \theta W_{2j} \\ W_{2j} &= -\sin \theta W_{1j} + \cos \theta W_{2j} \end{aligned} \quad (8)$$

III. THE COUPLED-CHANNEL DEPERTURBATION ANALYSIS OF THE $(1 \sim 2)^1\Pi$ COMPLEX

In the framework of the rigorous coupled-channel (CC) deperturbation model^{24,36,37}, the non-adiabatic rovibronic energy E^{CC} of the $(1,2)^1\Pi$ complex is determined by the solution of the two coupled radial equations

$$\begin{aligned} \left(-\mathbf{I} \frac{\hbar^2 d^2}{2\mu d R^2} + \mathbf{V}(R) - \mathbf{I} E^{CC} \right) \Phi(R) &= 0 \\ \Phi(0) = \Phi(\infty) &= 0, \end{aligned} \quad (9)$$

where μ is the reduced molecular mass, \mathbf{I} is the identity matrix and $\mathbf{V}(R)$ is the symmetric matrix of the potential energy given by

$$V_{1^1\Pi} = V_1; \quad V_{2^1\Pi} = V_2; \quad V_{1^1\Pi-2^1\Pi} = V_{12} \quad (10)$$

where the diabatic potentials $V_{1,2}(R)$ and electronic coupling matrix element $V_{12}(R)$ are the mass-invariant functions of internuclear distance R . The two-component

vibrational eigenfunction Φ in Eq.(9) is normalized for the bound states as $\sum_i P_i = 1$, where $P_i = \langle \phi_i | \phi_i \rangle$ ($i \in 1^1\Pi, 2^1\Pi$) is the fractional partition of the level with the energy E^{CC} .

The diabatic matrix elements are related to the adiabatic PECs as

$$U_{1,2} = (V_1 + V_2)/2 \pm \sqrt{(V_1 - V_2)^2/4 + V_{12}^2} \quad (11)$$

The corresponding "effective" rotational constant B^{CC} is defined as the expectation value

$$B^{CC} = \frac{\hbar^2}{2\mu} \sum_{i=1,2} \langle \phi_i | 1/R^2 | \phi_i \rangle \quad (12)$$

The rovibronic energies E^{CC} and vibrational wave functions $\phi_i(R)$ were obtained through solving the CC equations (9) by the finite-difference boundary value method³⁸. The adaptive analytical mapping procedure³⁹ was exploited to decrease the required number of grid points.

To perform a direct fit of the experimental data we represented the diabatic interatomic potentials and the relevant electronic coupling matrix element in their fully analytical forms. In particular, the Morse/Long-Range(MLR)⁴⁰⁻⁴² function

$$V_2(R) \equiv U_{MLR} = [T_2^{dis} - \mathfrak{D}_e] + \mathfrak{D}_e \left[1 - \frac{u_{LR}(R)}{u_{LR}(R_e)} e^{-\beta(R)y_p^{eq}(R)} \right]^2 \quad (13)$$

is used to approximate the diabatic PEC of the $2^1\Pi$ state converging to the $K(4^2S) + Rb(5^2P)$ dissociation threshold. The fixed parameter of the dissociation energy T_2^{dis} involved in Eq.(13) was determined as $T_2^{dis} = \mathfrak{D}_e^X + E_{Rb(5^2P)} - E_{Rb(5^2S)} = 16955.169 \text{ cm}^{-1}$, where the experimental dissociation energy of the ground state⁴³ (taken at the hfs center-of-gravity) $\mathfrak{D}_e^X = 4217.822 \text{ cm}^{-1}$ and the corresponding non-relativistic energy of the D -lines of the Rb atom²⁹.

The coefficient $\beta(R)$ in the MLR function

$$\beta_{MLR}(R) = y_p^{ref} \beta_\infty + [1 - y_p^{ref}] \sum_{i=0}^N \beta_i [y_q^{ref}]^i, \quad (14)$$

is the polynomial function of the reduced coordinates $y_{p,q}^{ref}$:

$$y_{p,q}^{ref}(R) = \frac{R^{p,q} - R_{ref}^{p,q}}{R^{p,q} + R_{ref}^{p,q}}, \quad (15)$$

where R_{ref} is the reference distance and the parameters q and p are integers. The reduced variable y_p^{ref} in Eq.(13) is defined by Eq.(15) where the R_{ref} is substituted for the equilibrium distance R_e . The parameter β_∞ is constrained to be $\ln\{2\mathfrak{D}_e/u_{LR}(R_e)\}$, where \mathfrak{D}_e is the well depth and u_{LR} is the long-range potential

$$u_{LR}(R) = \sum_{n=6,8} D_n \frac{C_n}{R^n} \quad (16)$$

with fixed sets of the dispersion coefficients C_n and the damping functions^{44,45} D_n :

$$D_n(R) = \left[1 - \exp \left(-\frac{3.3(\rho \cdot R)}{n} - \frac{0.423(\rho \cdot R)^2}{\sqrt{n}} \right) \right]^{n-1}, \quad (17)$$

where the scaling parameter $\rho = 0.461^{45}$.

To approximate the diabatic PEC of the $1^1\Pi$ state converging to the $K(4^2P) + Rb(5^2S)$ dissociation threshold we used the double-exponential/long-range (DELR) potential⁴⁶:

$$V_1(R) \equiv U_{DELR} = T_1^{dis} - u_{LR}(R) + \frac{Ae^{-2\beta(R)(R-R_e)} - Be^{-\beta(R)(R-R_e)}}{Ae^{-2\beta(R)(R-R_e)} - Be^{-\beta(R)(R-R_e)}} \quad (18)$$

which allowed us to represent a rotationless barrier above the third asymptote at distances $R > R_e$ (see, Fig. 1). The dissociation energy $T_1^{dis} = \mathfrak{D}_e^X + E_{K(4^2P)} - E_{K(4^2S)} = 17241.481 \text{ cm}^{-1}$ was fixed during the fit. The non-relativistic energy of the D -lines of the K atom was taken from Ref. 29.

The exponent coefficient $\beta(R)$ of the DELR potential was defined as

$$\beta_{DELR}(R) = \sum_{i=0}^N \beta_i [y_q^{ref}]^i \quad (19)$$

while the pre-exponential coefficients A and B were determined from the conditions $U_{DELR}(R_e) = 0$ and $dU_{DELR}/dR|_{R=R_e} = 0$ which lead to

$$\begin{aligned} A &= \mathfrak{D}_e - u_{LR}(R_e) - u'_{LR}(R_e)/\beta_{DELR}(R_e) \\ B &= \mathfrak{D}_e - u_{LR}(R_e) + A \end{aligned} \quad (20)$$

where $u'_{LR} \equiv du_{LR}/dR$.

Finally, the electronic coupling matrix element $V_{12}^{emp}(R)$ between the diabatic $1^1\Pi$ and $2^1\Pi$ states was represented by the polynomial:

$$V_{12}^{emp}(R) = (1 - y_q^{ref}) \sum_{i=0}^N \beta_i [y_q^{ref}]^i \quad (21)$$

The optimal parameters of the MLR and DELR potentials as well as electronic coupling matrix element were determined simultaneously in the framework of the weighted nonlinear least-squared fitting (NLSF) procedure:

$$\begin{aligned} \chi^2 &= \sum_{j=1}^{N^{exp}} (E_j^{exp} - E_j^{CC})/\sigma_j^{exp})^2 \\ &+ \sum_{j=1}^{N^{ab}} ([V_1^{ab}(R_j) - U_{DELR}(R_j)]/\sigma_j^{ab})^2 \\ &+ \sum_{j=1}^{N^{ab}} ([V_2^{ab}(R_j) - U_{MLR}(R_j)]/\sigma_j^{ab})^2 \\ &+ \sum_{j=1}^{N^{ab}} ([V_{12}^{ab}(R_j) - V_{12}^{emp}(R_j)]/\sigma_j^{ab})^2 \end{aligned} \quad (22)$$

where E_j^{exp} denote the experimental term values of the $(1 \sim 2)^1\Pi$ complex and the σ_j^{exp} -values mean their uncertainties. The $V_{1,2}^{ab}$ and V_{12}^{ab} are the diabatic functions evaluated by Eq.(5) at the point R_j , and σ_j^{ab} are their uncertainties obtained by averaging the present and preceding¹¹ *ab initio* curves. The theoretical curves were incorporated in the NLSF procedure in order to propagate the empirical functions outside of the experimental data region.

IV. RESULTS AND DISCUSSION

IV.1. Ab initio data

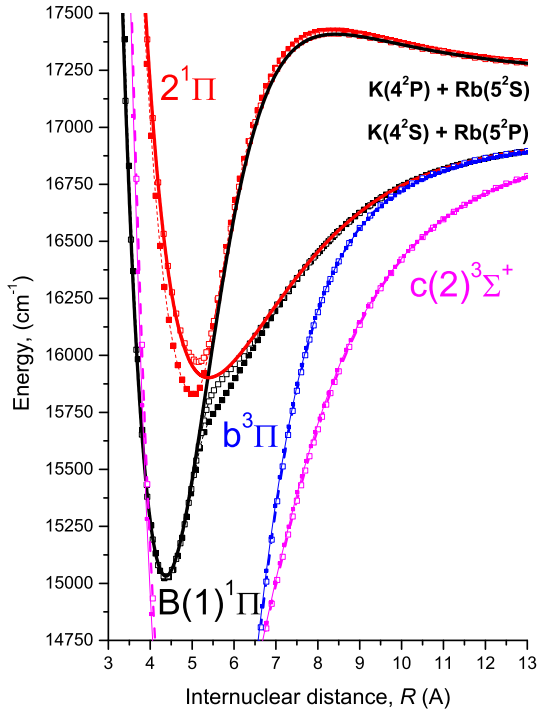


FIG. 3. The "difference-based" adiabatic PECs obtained from the present (open symbols) and preceding¹¹ (solid symbols) *ab initio* calculations. The solid lines denote the corresponding diabatic *ab initio* PECs of the $1^1\Pi$ and $2^1\Pi$ states.

The resulting "difference-based" PECs obtained by Eq.(6) for adiabatic $B(1)^1\Pi$ and $2^1\Pi$ states from the present and preceding¹¹ *ab initio* calculations demonstrates overall good agreement as can be seen in Fig. 3. The most significant deviations are observed in the vicinity of the avoided crossing point $R_c \approx 5.36$ (Å). The corresponding diabatic $V_1(R)$ and $V_2(R)$ PECs obtained by

the unitary transformation (5) are depicted as well.

The *ab initio* radial $B_{12}(R)$ and electronic $V_{12}(R)$ coupling matrix elements are given on Fig. 4a and b, respectively. The inset demonstrates that the simplest two-parameters Lorentz curve (3) perfectly fits a peak of the *ab initio* $B_{12}(R)$ function.

The permanent dipole moments of the $1^1\Pi$ and $2^1\Pi$ states as well as the corresponding $1^1\Pi - 2^1\Pi$ transition dipole moment are given on Fig. 5a. The adiabatic functions $d_{1,2}(R)$, $d_{12}(R)$ were obtained during the electronic structure calculations while the diabatic moments $\mu_{1,2}(R)$, $\mu_{12}(R)$ were evaluated according to Eq.(7). As follows from the charge density of the electronic wavefunctions of the twin $(1, 2)^1\Pi$ states¹⁹, the $d_{1,2}(R)$ functions have a "mirror" R -dependance $d_1 \approx -d_2$ with a sharp global extremum about ± 2 a.u. located near the point R_c . It should be noticed, that the adiabatic transition moment d_{12} becomes zero at the same point. In contrast to sharp adiabatic functions, their diabatic counterparts demonstrate rather smooth R -behavior. Furthermore, the absolute magnitudes of the diabatic $|\mu_{1,2}(R)|$ functions significantly decrease at intermediate internuclear distances.

The adiabatic $(1, 2)^1\Pi - (X, A)^1\Sigma^+$ transition dipole moments are depicted on Fig. 5b along with the diabatic moments evaluated by Eq.(8). A good agreement of the present $B(1)^1\Pi - X^1\Sigma^+$ transition moment and the preceding estimate²³ is observed. The Fig. 5b also shows that the diabatic $1^1\Pi - A^1\Sigma^+$ and $2^1\Pi \rightarrow X^1\Sigma^+$ moments are very small at short and intermediate R -distances.

The diabatic $1^1\Pi \rightarrow X^1\Sigma^+$ transition moment $\mu_{1X}(R)$ was used to evaluate a radiative lifetime for the lowest vibrational levels of the $1^1\Pi$ state by the approximate sum rule⁴⁷:

$$\frac{1}{\tau_{1^1\Pi}} \approx \frac{8\pi^2}{3\hbar\epsilon_0} \langle \phi_1^{J'} | [\Delta V_{1X}]^3 [\mu_{1X}]^2 | \phi_1^{J'} \rangle \quad (23)$$

where $\Delta V_{1X}(R) = V_1(R) - U_X(R)$ is the difference of the diabatic PEC of the $1^1\Pi$ state and ground state PEC. The resulting $\tau = 11.3$ ns predicted for the $B^1\Pi(v_1' = 2, J' = 41)$ level is remarkably close to its experimental counterpart¹³ of 11.6 ns. It should be noted, that the contribution of the $1^1\Pi - A^1\Sigma^+$ transition into the $\tau_{1^1\Pi}$ -estimate could be neglected since $|\mu_{1A}| \ll |\mu_{1X}|$ and $|\Delta V_{1A}| \ll |\Delta V_{1X}|$.

The resulting SOC matrix elements obtained during the present *ab initio* calculations are depicted on Fig. 6. As expected, the diabaticization procedure provides a smooth R -behavior of most SOC functions. However, the diabatic $(1, 2)^1\Pi - 3^3\Sigma^+$ functions are still not smooth enough since the radial coupling of the $3^3\Sigma^+$ state with the higher ($n \geq 4$) $3^3\Sigma^+$ states takes place. It should be also noted that the present $B^1\Pi - c^3\Sigma^+$ and $B^1\Pi - b^3\Pi$ functions deviate significantly at short and intermediate R -ranges from the preceding result⁶, which has been used in modeling the optimal $a^3\Sigma^+ \rightarrow B^1\Pi \sim c^3\Sigma^+ \rightarrow X^1\Sigma^+$ STIRAP cycle⁷.

The angular coupling matrix elements $L_{ij}^{\pm}(R)$ obtained for the $(1,2)^1\Pi - (1-3)^1\Sigma^+$ non-adiabatic transitions are presented on Fig. 7. It is seen that Van Vleck's *pure precession* hypothesis³⁰ $L_{ij}^{\pm} \approx \sqrt{l(l+1)} = \text{const}$ works perfectly for the $1^1\Pi - A^1\Sigma^+$ pair with $l = 1$. With $l = 2$, it works fairly well for the $2^1\Pi - 3^1\Sigma^+$ pair at short and intermediate distances.

Under *unique perturber* approximation³⁰ the q -factors of the doubly degenerate $1^1\Pi$ states are estimated as

$$q_{1\Pi} \approx \left(\frac{\hbar^2}{2\mu R_e^2} \right)^2 \sum_{1\Sigma^+} \frac{2l(l+1)}{T_e^{1\Pi} - T_e^{1\Sigma^+}} \quad (24)$$

yielding, for the $^{39}\text{K}^{85}\text{Rb}$ diabatic states, $q_{1^1\Pi} \approx 3.2 \times 10^{-5}$ and $q_{2^1\Pi} \approx 1.5 \times 10^{-4} \text{ cm}^{-1}$, respectively. Unfortunately, there are no experimental q -values for comparison so far.

The resulting *ab initio* potential energy curves, permanent and transition dipole moments as well as electronic, spin-orbit and angular coupling matrix elements are given in pointwise form in the Supplementary material⁴⁸.

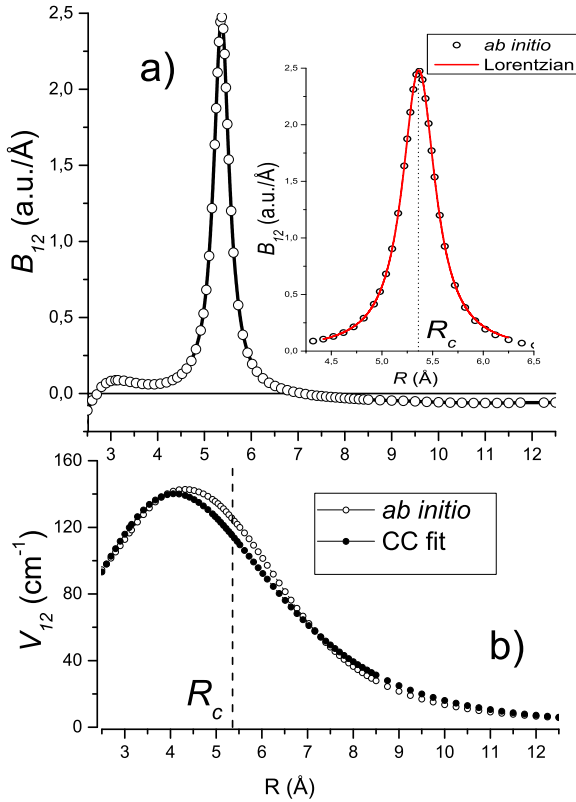


FIG. 4. (a) The radial coupling electronic matrix element $B_{12}(R)$ calculated between adiabatic $1^1\Pi$ and $2^1\Pi$ states. On the inset the red line depicts the fitting Lorentz curve (3) with the parameters $R_c = 5.36$ and $w = 0.4036$ (both in Å). (b) The *ab initio* and empirical electronic coupling $V_{12}(R)$ function between diabatic $1^1\Pi$ and $2^1\Pi$ states.

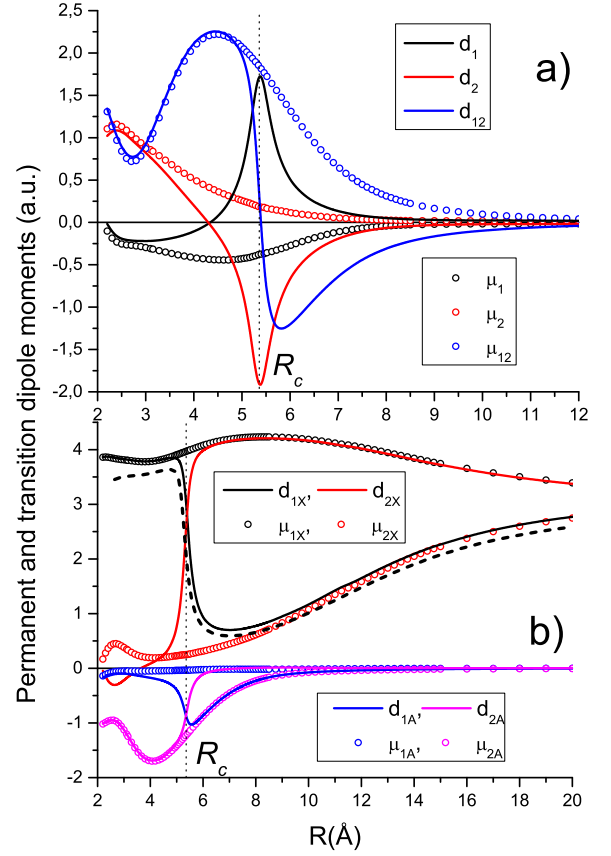


FIG. 5. (a) The adiabatic and diabatic *ab initio* permanent dipole moments of the $1^1\Pi$ and $2^1\Pi$ states as well as the corresponding $1^1\Pi - 2^1\Pi$ transition moment. (b) The *ab initio* TDM functions between the $(1,2)^1\Pi$ and $X, A^1\Sigma^+$ states. The dashed line denotes the adiabatic $d_{B^1\Pi-X^1\Sigma^+}(R)$ function from Ref. 23.

IV.2. CC deperturbation data

Experimental input data of the $1^1\Pi \sim 2^1\Pi$ complex used in the NLSF fitting procedure (22) consists of (i) the 110 original rovibronic termvalues¹⁶ $E_{v',J'}^{exp}$ obtained during the $(3)^1\Pi \rightarrow (1,2)^1\Pi$ FTS LIF experiment¹⁵ for the rotational levels $J' \in [24, 145]$ in the short range of vibrational quantum numbers $v'_1, v'_2 \in [0, 6]$; (ii) the reduced termvalues $E_{v'}^{exp}$ obtained by the OODRPS measurements^{13,14} for the $v'_1 \in [0, 69]$ and $v'_2 \in [6, 19]$ levels, respectively; (iii) the rotationless ($J' = 0$) termvalues extracted from the MB experiment¹⁷ for $v'_1 \in [0, 20]$ levels.

All energies above correspond to the most abundant $^{39}\text{K}^{85}\text{Rb}$ isotopologue while the 29 rovibronic termvalues¹⁶ of $^{39}\text{K}^{87}\text{Rb}$ held in reserve for confirmation of the mass-invariant properties of the fitting functions. The uncertainty σ^{exp} of the raw rovibronic termvalues¹⁶ was taken as 0.05 cm^{-1} while the $\sigma^{exp} = 2 \text{ cm}^{-1}$ was adopted for the vibronic terms $E_{v'}^{exp}$ since the difference of the empirical data^{13,14} and Ref. 17 reach few reciprocal cen-

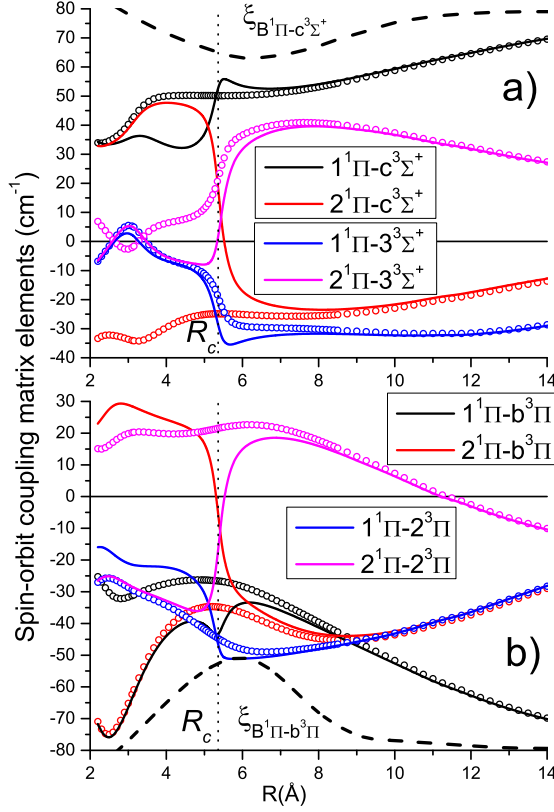


FIG. 6. The adiabatic (solid lines) and diabatic (open circles) *ab initio* spin-orbit coupling matrix elements $\xi_{ij}(R)$ between the $(1,2)^1\Pi$ and $(2,3)^3\Sigma^+$ (a), $(1,2)^3\Pi$ (b) states. The dashed lines denote the adiabatic $\xi_{B^1\Pi\text{-}c^3\Sigma^+}(R)$ and $\xi_{B^1\Pi\text{-}b^3\Pi}(R)$ SOC functions borrowed from Ref. 6.

timeters (see, Fig. 8b).

The adjusted mass-invariant parameters of the DELR (18) and MLR (13) potentials obtained for the diabatic $1^1\Pi$ and $2^1\Pi$ states are presented on Table II and III, respectively. The fitting parameters of the empiric $1^1\Pi \sim 2^1\Pi$ coupling function (21) are given on the Table IV. The resulting parameters are duplicated in non-truncated ASCII form in the Supplementary material⁴⁸, where both experimental and CC term values along with their residuals (see Fig. 8) and fractional partitions are collected as well. The adiabatic PECs obtained by the transformation (11) from the empirical diabatic functions agree very well with the corresponding RKR potentials in the low energy region (see Fig. 2).

Fig. 8a demonstrates that the present deperturbation model allows one to reproduce the most experimental rovibronic termvalues¹⁶ of the $^{39}\text{K}^{85}\text{Rb}$ isotopologue and to predict the $E_{v',J'}^{\text{exp}}$ -values of the $^{39}\text{K}^{87}\text{Rb}$ isotopologue with an uncertainty close to 0.05 cm^{-1} . However, there are several pronounced deviations of the experimental termvalues corresponding to the particular rotational levels of $v'_1 = 4, 5$ vibrational states from the CC estimates

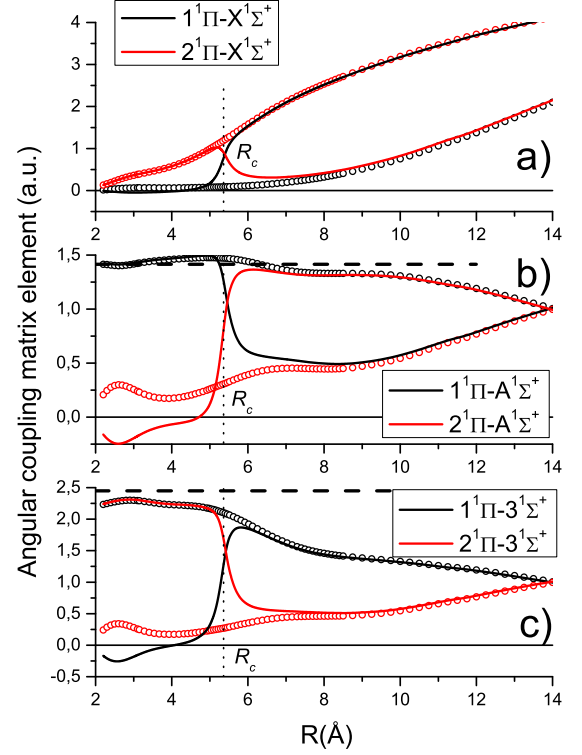


FIG. 7. The adiabatic (solid lines) and diabatic (open circles) *ab initio* angular coupling matrix elements $L_{ij}^\pm(R)$ calculated between the $(1,2)^1\Pi$ and $X^1\Sigma^+$ (a), $A^1\Sigma^+$ (b), $3^1\Sigma^+$ (c) states. The horizontal dashed lines correspond to $\sqrt{2}$ (b) and $\sqrt{6}$ (c) values, respectively.

(see the Supplementary material⁴⁸ for details). The observed outliers are attributed to the local SOC effect with the lower lying $c(2)^3\Sigma^+$ state (see, Fig. 3).

The CC diabatic model also improves the representation of the vibronic $E_{v',J'}^{\text{exp}}$ termvalues^{13,14,17} up to the excitation energies $\sim 16400 \text{ cm}^{-1}$ (see Fig. 8b). Overall good agreement of the calculated $B_{v',J'}^{CC}$ (12) and empirical $B_{v',J'}^{\text{exp}}$ rotational constants is observed on Fig. 9 for the vibrational $v'_1 \leq 40$ and $v'_2 \leq 6$ levels.

To test extrapolation possibilities of the deperturbation model we have calculated rovibronic termvalues $E_{v',J'}^{CC}$ for a pair of the closely lying $1^1\Pi(v'_1 = 54) \sim 2^1\Pi(v'_2 = 15)$ levels of the $(1 \sim 2)^1\Pi$ complex (see Fig. 10) experimentally studied in Ref. 14. The vibrational numbering used above corresponds to the adiabatic representation of the $1^1\Pi \sim 2^1\Pi$ complex applied for the assignment of the OODRPS $X^1\Sigma^+ \rightarrow 1^1\Pi \sim 2^1\Pi$ spectra¹⁴. The calculated $E_{v',J'}^{CC}$ positions are found to be in a good agreement with their experimental counterparts. In particular, the minimal distance $\Delta^{CC} = 4.3 \text{ cm}^{-1}$ predicted at $J' = 27$ is remarkably close to the empirical estimate $\Delta^{\text{exp}} = 2 \times 2.2 \text{ cm}^{-1}$ obtained in Ref. 14. The

fraction partition $P_{ki} \equiv \langle \phi_{ki}^{J'} | \phi_{ki}^{J'} \rangle$ of the CC vibrational eigenfunctions highlights a strong dependance of admixture of states on the rotational quantum number in the interval $J' \in [11, 35]$.

The divergence of the present CC estimates and empirical band constants generally increases as the vibrational excitation increases (see Fig. 8c). The same effect takes places in the empirical adiabatic PECs and RKR potentials. It can be attributed to the monotonically growing SO coupling with the $b^3\Pi$ state correlated with the same dissociation limit (see, Fig. 3). Furthermore, the high vibrational $1^1\Pi(v'_1 \geq 63)$ levels lying just above the fine $4^2S_{1/2}(K) + 5^2P_{1/2}(Rb)$ asymptotic undergo a predissociation effect¹⁴.

Thus, raw experimental termvalues corresponding to high v', J' -levels of the $(1 \sim 2)^1\Pi$ complex would be certainly useful for the comprehensive deperturbation analysis since the "effective" band constants indispensably "absorb" the spin-orbit perturbation effect in the high energy region.

TABLE II. The resulting mass-invariant parameters of the $U_{DELR}(R)$ potential (18) obtained for the diabatic $1^1\Pi$ state.

fitted	
$\mathfrak{D}_e, \text{cm}^{-1}$	2214.757
$R_e, \text{\AA}$	4.3715
A, cm^{-1}	-10280.36
B, cm^{-1}	4577.51
$\beta_0, \text{\AA}^{-1}$	0.47730
$\beta_1, \text{\AA}^{-1}$	0.22714
$\beta_2, \text{\AA}^{-1}$	0.11574
$\beta_3, \text{\AA}^{-1}$	-0.04563
$\beta_4, \text{\AA}^{-1}$	-0.20030
$\beta_5, \text{\AA}^{-1}$	0.19131
$\beta_6, \text{\AA}^{-1}$	0.73518
$\beta_7, \text{\AA}^{-1}$	-0.15280
$\beta_8, \text{\AA}^{-1}$	-0.72517
fixed	
q	3
$R_{ref}, \text{\AA}$	5.6781
T^{dis}, cm^{-1}	17241.481
$C_6, \text{cm}^{-1} \cdot \text{\AA}^6$	-2339×10^5
$C_8, \text{cm}^{-1} \cdot \text{\AA}^8$	9536×10^5

IV.3. Intensity anomalies of the

$X^1\Sigma^+(v'' = 12) \rightarrow 1^1\Pi(v' = 54) \sim 2^1\Pi(v' = 15)$ transition

The present deperturbation model (9) combined with diabatic $(1, 2)^1\Pi - X^1\Sigma^+$ transition moments $\mu_{1X}(R)$, $\mu_{2X}(R)$ (see Fig. 5b) was used to elucidate the "abnormal" intensity distribution observed for the $X^1\Sigma^+(v''_X = 12, J'' = J' + 1) \rightarrow 1^1\Pi(v'_1 = 54, J') \sim 2^1\Pi(v'_2 = 15, J')$ rovibronic transition¹⁴.

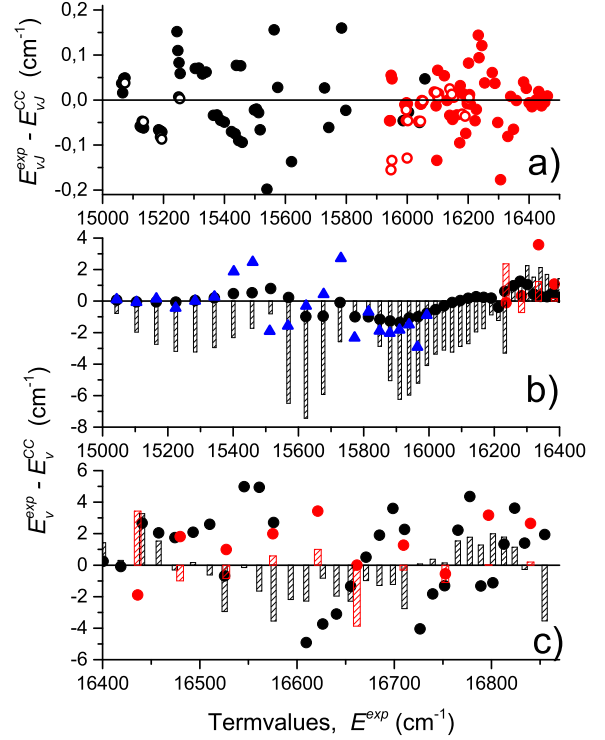


FIG. 8. The residual of the experimental termvalues of the $1^1\Pi \sim 2^1\Pi$ complex and CC estimates (9). Black and red circles mark the $1^1\Pi$ and $2^1\Pi$ states, respectively. (a) Solid symbols correspond to the rovibronic termvalues¹⁶ of $^{39}\text{K}^{85}\text{Rb}$ isotopologue while open circles - $^{39}\text{K}^{87}\text{Rb}$. (b-c) The circles denote the OODRPS termvalues^{13,14} while the triangles denote the MB data¹⁷. The bars denotes the differences between the empirical terms and their estimates evaluated by the corresponding RKR potentials.

The absorption intensities from the ground $X^1\Sigma^+$ state to a pair of adjoining levels of the $(1 \sim 2)^1\Pi$ complex were evaluated according to the relation:

$$I_{k^1\Pi-X^1\Sigma^+}^{CC} \sim |M_{kX}|^2 \quad (25)$$

$$= |\langle \phi_{k1}^{J'} | \mu_{1X} | \chi_X^{J''} \rangle|^2 + |\langle \phi_{k2}^{J'} | \mu_{2X} | \chi_X^{J''} \rangle|^2$$

$$+ 2\langle \phi_{k1}^{J'} | \mu_{1X} | \chi_X^{J''} \rangle \langle \phi_{k2}^{J'} | \mu_{2X} | \chi_X^{J''} \rangle$$

where $k = 1, 2$ is the index of the states represented on Fig. 10, $\phi_{k1}^{J'}(R)$, $\phi_{k2}^{J'}(R)$ are the CC rovibrational wavefunctions and $\chi_X^{J''}(R)$ are the vibrational wavefunctions of the ground X -state (see Fig. 11) calculated with the highly accurate empirical potential¹⁸.

The rovibronic $\langle \phi_{k1}^{J'} | \mu_{1X} | \chi_X^{J''} \rangle$ and $\langle \phi_{k2}^{J'} | \mu_{2X} | \chi_X^{J''} \rangle$ matrix elements calculated for the $X^1\Sigma^+(v''_X = 12) \rightarrow 1^1\Pi(v'_1 = 54) \sim 2^1\Pi(v'_2 = 15)$ transitions are given on Fig. 12a. It is seen that the $\langle \phi_{k2}^{J'} | \mu_{2X} | \chi_X^{J''} \rangle$ terms give a negligible contribution to the total $|M_{kX}|^2$ transition

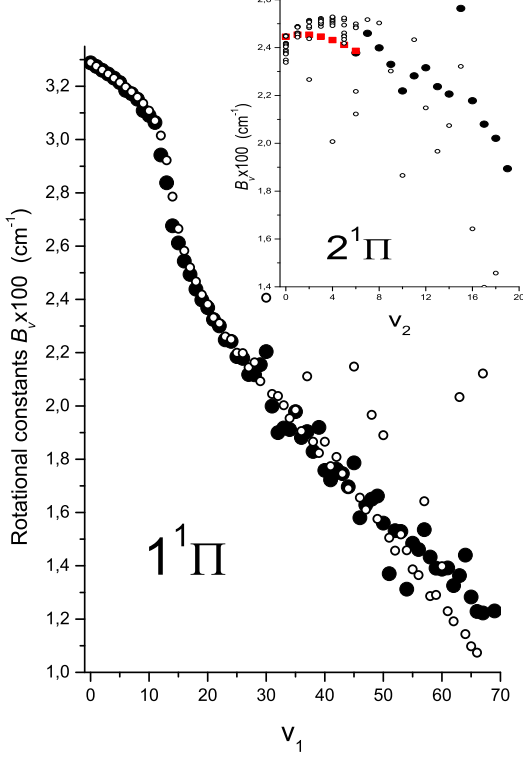


FIG. 9. Comparison of the empirical (solid circles) rotational constants $B_{v'}^{exp}$ of the $1^1\Pi \sim 2^1\Pi$ complex^{13,14} and theoretical $B_{v'}^{CC}$ estimates (open circles) derived by Eq.(12). Red squares on the inset denote $B_{v'}^{exp}$ -values calculated for the $v_2' \leq 6$ levels by the Dunham constants¹⁵.

TABLE III. The resulting mass-invariant parameters of the $U_{MLR}(R)$ (13) potential obtained for the diabatic $2^1\Pi$ state.

fitted	
$\mathcal{D}_e, \text{cm}^{-1}$	1111.961
$R_e, \text{\AA}$	5.2872
β_0	-0.92350
β_1	0.09744
β_2	0.09023
β_3	-0.71368
β_4	-1.08251
β_5	0.12502
β_6	0.35828
fixed	
q	4
p	4
$R_{ref}, \text{\AA}$	6.8511
T^{dis}, cm^{-1}	16955.169
$C_6, \text{cm}^{-1} \cdot \text{\AA}^6$	3025×10^5
$C_8, \text{cm}^{-1} \cdot \text{\AA}^8$	7875×10^5

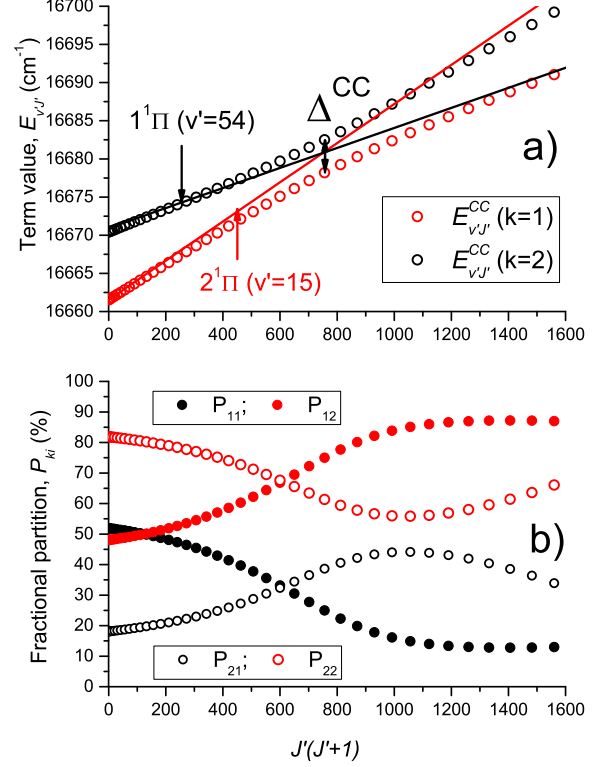


FIG. 10. (a) The rovibronic termvalues $E_{v',J'}^{CC}$ predicted for the $1^1\Pi(v' = 54) \sim 2^1\Pi(v' = 15)$ levels under the present CC deperturbation model. The straight lines denotes the adiabatic energies calculated as $E_{v'}^{exp} + B_{v'}^{exp} \times J'(J' + 1)$ by the "effective" band constants¹⁴. The symbol Δ^{CC} means the minimal distance predicted at $J' = 27$. (b) The fraction partition P_{ki} of the CC eigenfunctions corresponding to term-values above.

TABLE IV. The resulting mass-invariant parameters of the electronic $1^1\Pi \sim 2^1\Pi$ coupling $V_{12}^{emp}(R)$ function (21).

fitted	
β_0	114.87
β_1	-2.4087
β_2	-98.392
fixed	
q	3
$R_{ref}, \text{\AA}$	5.36

probability since $|\mu_{2X}| \ll |\mu_{1X}|$ (see Fig. 5b). Furthermore, $\langle \phi_{21}^{J'} | \mu_{1X} | \chi_X^{J''} \rangle$ matrix elements demonstrate abnormally strong J' -dependance, and they accidentally become very small in the vicinity of $J' \approx 25$ due to the interference effect taking place in the overlap integral of the upper and ground rovibrotional wavefunctions.

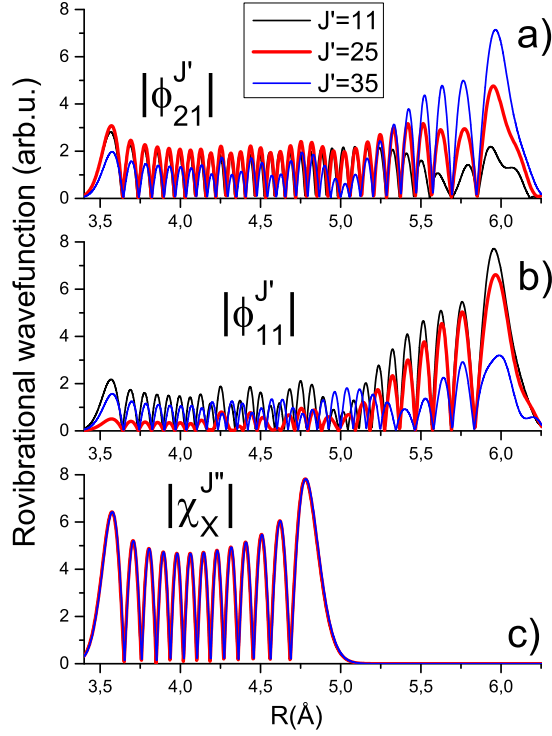


FIG. 11. The nodal structure of vibrational wavefunctions calculated for the particular rotational $J' = J'' - 1$ levels of the upper $v'_1 = 54$ (a), $v'_2 = 15$ (b) and ground $v''_X = 12$ (c) vibrational states.

V. CONCLUDING REMARKS

We performed the diabaticization of the twin $(1,2)^1\Pi$ states of KRb based on an *ab initio* electronic structure calculation and the direct coupled-channel treatment of experimental term values of the $(1 \sim 2)^1\Pi$ complex. The present CC deperturbation model, based on a diabatic representation, provides the almost spectroscopic (experimental) accuracy of the approximation. The empirical PECs and electronic coupling function, along with *ab initio* spin-orbit and angular coupling matrix elements, could be utilized in further deperturbation analysis carried out in the framework of both adiabatic and diabatic approximation. The diabatic transition dipole moments are appropriated for radiative property estimates.

ACKNOWLEDGMENTS

Authors are indebted to Claude Amiot for providing the raw rovibronic termvalues of the $(1 \sim 2)^1\Pi$ complex and Ekaterina Bormotova for fruitful discussion. The work was partly supported by RFBR grant No. 16-03-

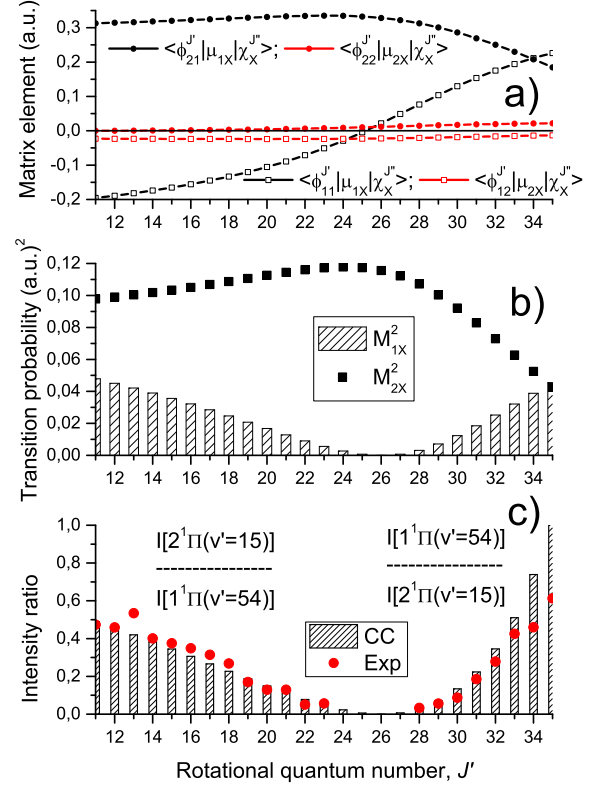


FIG. 12. (a) The rovibronic transition matrix elements calculated for the $v''_X = 12 \rightarrow v'_1 = 54 \sim v'_2 = 15$ transition; (b) The total $X^1\Sigma^+ \rightarrow 1^1\Pi \sim 2^1\Pi$ transition probabilities; (c) Comparison of the theoretical (25) and experimental¹⁴ intensity ratios. The experimental points were digitized from Fig.8 of Ref. 14.

00529a.

REFERENCES

- ¹R. Krems, B. Friedrich, and W. C. Stwalley, *Cold molecules: theory, experiment, applications* (CRC press, 2009).
- ²E. A. Pazyuk, A. V. Zaitsevskii, A. V. Stolyarov, M. Tamanis, and R. Ferber, *Russ. Chem. Rev.* **84**, 1001 (2015).
- ³K. Bergmann, N. V. Vitanov, and B. W. Shore, *J. Chem. Phys.* **142**, 170901 (2015).
- ⁴D. Wang, J. Qi, M. Stone, O. Nikolayeva, H. Wang, B. Hattaway, S. Gensemer, P. Gould, E. Eyler, and W. Stwalley, *Phys. Rev. Lett.* **93**, 243005 (2004).
- ⁵W. Stwalley, J. Banerjee, M. Bellos, R. Carollo, M. Recore, and M. Mastroianni, *J. Phys. Chem. A* **114**, 81 (2010).
- ⁶S. Kotochigova, E. Tiesinga, and P. S. Julienne, *New J Phys* **11**, 055043 (2009).
- ⁷D. Borsalino, B. Londoño-Florèz, R. Vexiau, O. Dulieu, N. Bouloufa-Maafa, and E. Luc-Koenig, *Phys. Rev. A* **90**, 033413 (2014).
- ⁸J.-T. Kim, Y. Lee, B. Kim, D. Wang, W. C. Stwalley, P. L. Gould, and E. E. Eyler, *Phys. Rev. A* **84**, 062511 (2011).

- ⁹K.-K. Ni, S. Ospelkaus, D. Wang, G. Quémener, B. Neyenhuis, M. De Miranda, J. Bohn, J. Ye, and D. Jin, *Nature* **464**, 1324 (2010).
- ¹⁰K. Aikawa, D. Akamatsu, M. Hayashi, K. Oasa, J. Kobayashi, P. Naidon, T. Kishimoto, M. Ueda, and S. Inouye, *Phys. Rev. Lett.* **105**, 203001 (2010).
- ¹¹S. Rousseau, A. Allouche, and M. Aubert-Frécon, *J. Mol. Spectrosc.* **203**, 235 (2000).
- ¹²J.-T. Kim, B. Kim, and W. C. Stwalley, *Analysis of the Alkali Metal Diatomic Spectra* (Morgan & Claypool Publishers, 2014).
- ¹³N. Okada, S. Kasahara, T. Ebi, M. Baba, and H. Katô, *J. Chem. Phys.* **105**, 3458 (1996).
- ¹⁴S. Kasahara, C. Fujiwara, N. Okada, H. Katô, M. Baba, *et al.*, *J. Chem. Phys.* **111**, 8857 (1999).
- ¹⁵C. Amiot, J. Verges, C. Effantin, and J. d’Incan, *Chem. Phys. Lett.* **321**, 21 (2000).
- ¹⁶C. Amiot, private communication (2016).
- ¹⁷J.-T. Kim, Y. Lee, B. Kim, D. Wang, W. C. Stwalley, P. L. Gould, and E. E. Eyler, *Phys. Chem. Chem. Phys.* **13**, 18755 (2011).
- ¹⁸A. Pashov, O. Docenko, M. Tamanis, R. Ferber, H. Knöckel, and E. Tiemann, *Phys. Rev. A* **76**, 022511 (2007).
- ¹⁹T. Leininger and G.-H. Jeung, *Phys. Rev. A* **51**, 1929 (1995).
- ²⁰T. Leininger, H. Stoll, and G.-H. Jeung, *J. Chem. Phys.* **106**, 2541 (1997).
- ²¹A. Yiannopoulou, T. Leininger, A. M. Lyyra, and G.-H. Jeung, *International Journal of Quantum Chemistry* **57**, 575 (1996).
- ²²S. J. Park, Y. J. Choi, Y. S. Lee, and G.-H. Jeung, *Chem. Phys.* **257**, 135 (2000).
- ²³R. Beuc, M. Movre, T. Ban, G. Pichler, M. Aymar, O. Dulieu, and W. E. Ernst, *J. Phys. B: Atom. Mol. Phys.* **39**, S1191 (2006).
- ²⁴K. Alps, A. Kruzins, M. Tamanis, R. Ferber, E. A. Pazyuk, and A. V. Stolyarov, *J. Chem. Phys.* **144**, 144310 (2016).
- ²⁵M. Shundalau, G. Pitsevich, A. Malevich, A. Hlinisty, A. Minko, R. Ferber, and M. Tamanis, *Computational and Theoretical Chemistry* **1089**, 35 (2016).
- ²⁶S. Kotochigova, P. Julienne, and E. Tiesinga, *Phys. Rev. A* **68**, 022501 (2003).
- ²⁷A. A. Radzig and B. M. Smirnov, *Reference data on atoms, molecules, and ions*, Vol. 31 (Springer Science & Business Media, 2012).
- ²⁸J. Mitroy, M. S. Safronova, and C. W. Clark, *J. Phys. B: Atom. Mol. Phys.* **43**, 202001 (2010).
- ²⁹A. Kramida, Yu. Ralchenko, J. Reader, and NIST ASD Team, NIST Atomic Spectra Database (ver. 5.3): <http://physics.nist.gov/asd>. National Institute of Standards and Technology, Gaithersburg, MD.
- ³⁰H. Lefebvre-Brion and R. W. Field, *The Spectra and Dynamics of Diatomic Molecules* (Academic Press, 2004).
- ³¹H.-J. Werner, P. J. Knowles, G. Knizia, F. R. Manby, M. Schütz, *et al.*, “Molpro, version 2010.1, a package of ab initio programs,” (2010), see <http://www.molpro.net/>.
- ³²I. S. Lim, P. Schwerdtfeger, B. Metz, and H. Stoll, *J. Chem. Phys.* **122**, 104103 (2005).
- ³³H.-J. Werner and P. J. Knowles, *J. Chem. Phys.* **82**, 5053 (1985).
- ³⁴P. J. Knowles and H.-J. Werner, *Theor. Chim. Acta* **84**, 95 (1992).
- ³⁵I. S. Lim, W. C. Lee, Y. S. Lee, and G.-H. Jeung, *J. Chem. Phys.* **124**, 234307 (2006).
- ³⁶T. Bergeman, C. Fellows, R. Gutterres, and C. Amiot, *Phys. Rev. A* **67**, 050501 (2003).
- ³⁷V. V. Meshkov, E. A. Pazyuk, A. Zaitsevskii, A. V. Stolyarov, R. Brühl, and D. Zimmermann, *J. Chem. Phys.* **123**, 204307 (2005).
- ³⁸S. N. Yurchenko, L. Lodi, J. Tennyson, and A. V. Stolyarov, *Comp. Phys. Comm.* **202**, 262 (2016).
- ³⁹V. V. Meshkov, A. V. Stolyarov, and R. J. Le Roy, *Phys. Rev. A* **78**, 052510 (2008).
- ⁴⁰R. J. Le Roy, Y. Huang, and C. Jary, *J. Chem. Phys.* **125**, 164310 (2006).
- ⁴¹R. J. Le Roy and R. D. E. Henderson, *Mol. Phys.* **105**, 663 (2007).
- ⁴²H. Salami, A. J. Ross, P. Crozet, W. Jastrzebski, P. Kowalczyk, and R. J. Le Roy, *J. Chem. Phys.* **126**, 194313 (2007).
- ⁴³D. Wang, J.-T. Kim, C. Ashbaugh, E. Eyler, P. Gould, and W. Stwalley, *Phys. Rev. A* **75**, 032511 (2007).
- ⁴⁴R. J. Le Roy, N. S. Dattani, J. A. Coxon, A. J. Ross, P. Crozet, and C. Linton, *J. Chem. Phys.* **131**, 204309 (2009).
- ⁴⁵R. J. Le Roy, C. C. Haugen, J. Tao, and H. Li, *Mol. Phys.* **109**, 435 (2011).
- ⁴⁶Y. Huang and R. J. Le Roy, *J. Chem. Phys.* **119**, 7398 (2003).
- ⁴⁷E. A. Pazyuk, A. V. Stolyarov, and V. I. Pupyshev, *Chem. Phys. Lett.* **228**, 219 (1994).
- ⁴⁸See EPAPS Document No. ... for data files associated with this paper. This document can be reached via a direct link in the online article’s HTML reference section or via the EPAPS homepage (<http://www.aip.org/pubservs/epaps.html>).